

# Nanoscale

Accepted Manuscript



This is an *Accepted Manuscript*, which has been through the Royal Society of Chemistry peer review process and has been accepted for publication.

*Accepted Manuscripts* are published online shortly after acceptance, before technical editing, formatting and proof reading. Using this free service, authors can make their results available to the community, in citable form, before we publish the edited article. We will replace this *Accepted Manuscript* with the edited and formatted *Advance Article* as soon as it is available.

You can find more information about *Accepted Manuscripts* in the [Information for Authors](#).

Please note that technical editing may introduce minor changes to the text and/or graphics, which may alter content. The journal's standard [Terms & Conditions](#) and the [Ethical guidelines](#) still apply. In no event shall the Royal Society of Chemistry be held responsible for any errors or omissions in this *Accepted Manuscript* or any consequences arising from the use of any information it contains.

# Detection and Characterization of Nanoparticles in Suspension at Low Concentrations Using the X-ray Total Scattering Pair Distribution Function Technique

Maxwell W. Terban,<sup>a</sup> Matthew Johnson,<sup>b‡</sup> Marco Di Michiel,<sup>c</sup> and Simon J. L. Billinge<sup>\*a,d</sup>

Received Xth XXXXXXXXXXXX 20XX, Accepted Xth XXXXXXXXXXXX 20XX

First published on the web Xth XXXXXXXXXXXX 200X

DOI: 10.1039/b000000x

Difference atomic pair distribution function methods have been applied to detect and characterize nanoparticles suspended in a solvent at very dilute concentrations. We specifically consider nanoparticles of a pharmaceutical compound in aqueous solution using X-ray PDF methods, a challenging case due to the low atomic number of the nanoparticle species. The nanoparticles were unambiguously detected at the level of 0.25 wt. %. Even at these low concentrations the signals were highly reproducible, allowing for reliable detection and quantitative analysis of the nanoparticle structure.

## 1 Introduction

Many modern material systems contain heterogenous mixtures of components, including nanometer scale particles and structures. It is important to be able to characterize the structures of the components in such complex mixtures. For example, colloidal dispersions of nanoparticles in solvent have garnered attention for their usefulness in developing a more fundamental understanding of nanoparticle synthesis,<sup>1</sup> along with direct applications in drug delivery,<sup>2</sup> imaging,<sup>3</sup> coatings,<sup>4</sup> food processing,<sup>5</sup> industrial fluids,<sup>6</sup> and the development of self-assembling materials and superstructures,<sup>7,8</sup> to name just a few. It is often desirable to work with very low concentrations, whether to achieve the proper pharmacokinetic properties of a drug molecule or to prevent particle aggregation and settling. Techniques such as SAXS, UV-Vis,<sup>9</sup> DLS,<sup>10</sup> and even TEM,<sup>11</sup> have been used *in situ* to quantify particle count and morphology but become increasingly challenging at lower concentrations. Meanwhile, quantitative structural analysis of the very particles themselves remains elusive.

Atomic pair distribution function (PDF) analysis of total scattering data is an effective technique for studying structure in such systems.\* It uses both Bragg and diffuse scattering to

obtain the scaled probability of finding two atoms in a material a distance  $r$  apart relative to the average atom-pair density of the material.<sup>12</sup> Information regarding physical and chemical properties of the local structure can be obtained from this. Lacking the necessary presumption of infinite periodicity, it has lent success to quantitative analysis of nanoparticle structure and dynamics,<sup>13–16</sup> stacking defects and size induced strain states,<sup>17–19</sup> and even *ab initio* structure determination,<sup>20</sup> with output in these directions growing rapidly. These advantages have recently extended the technique toward *systems* of ingredients. Here, difference atomic pair distribution function (dPDF) methods are often used, in which a signal from only the component of interest is extracted by subtracting scattering contributions from other components, background, and environment. Studies using this method have included multi-component systems such as mixed crystalline and amorphous phases,<sup>21–24</sup> adsorbent and adsorbate components in surface interaction studies,<sup>25–28</sup> and guest-host structures.<sup>29–32</sup> *In situ* studies using dPDF analysis are also becoming more popular in order to extract information about materials in their working environments at functionally relevant conditions; these have included nanoparticle studies of formation,<sup>1,33–38</sup> phase transformations,<sup>39,40</sup> and reaction chemistry,<sup>41–44</sup> including *in operando* studies of devices at work.<sup>45,46</sup> Note that the difference PDF approaches described here should not be confused with separate differential PDF methods which instead take advantage of X-ray anomalous scattering, the so-called differential anomalous pair distribution function approach.<sup>12,47,48</sup>

It is important to determine the sensitivity of the dPDF method to the concentration of constituents of interest, for

<sup>a</sup> Department of Applied Physics and Applied Mathematics, Columbia University, New York, NY 10027, USA.

<sup>b</sup> GlaxoSmithKline Medicines Research Centre, Gunnels Wood Road, Stevenage, Hertfordshire, SG1 2NY, UK.

<sup>‡</sup> Present address: Science and Technologies Facilities Council, Polaris House, North Star Avenue, Swindon, SN2 1SZ, UK.

<sup>c</sup> ESRF - The European Synchrotron, CS40220, 38043 Grenoble Cedex 9, France.

<sup>d</sup> Condensed Matter Physics and Materials Science Department, Brookhaven National Laboratory, Upton, NY 11973, USA. E-mail: sb2896@columbia.edu

\* The PDF referred to here is often called the TSPDF in the pharmaceutical literature

example, studies of minute impurity phases in solids, or in this case, nanoparticles in solution. This value is dependent upon species scattering intensity, structural arrangement (e.g. whether the signal is crystalline or amorphous), and measured counting statistics, so defining a generic limit is imprecise. Concentrations at and above 1 wt. % are widely quoted, for example 2.5 wt. % amorphous in crystalline silica,<sup>22</sup> and 1 wt. % platinum nanoparticles on alumina support.<sup>42</sup> Sensitivity down to 0.2 wt. % is reported for CdSe nanoparticles in toluene.<sup>49</sup> Here, the sensitivity is measured to 0.25 wt. %, but in this case for an organic sample which has a much weaker scattering power than the prior cases. The practicality of such measurements is improved by taking advantage of data reduction methods used by the software PDFGETX3.<sup>50</sup> This is for a system of organic nanoparticles in an aqueous suspension, which is an extremely challenging case due to the weaker scattering of the particles of interest. Samples consisted of small nanoparticles of a proprietary active pharmaceutical ingredient (API) under development by GlaxoSmithKline.

## 2 Results and Discussion

Samples included the API as a bulk crystalline powder and as precipitated from a non-microfluidized 5 wt. % suspension (2 % Polysorbate 80 (PS80), 0.2 % Sorbitan monolaurate (SML), 0.3 % Oleic Acid (OA) in water), three samples of API in the same solution at concentrations of 5, 0.66, and 0.25 wt. % which were size reduced by microfluidization, and a blank sample of the aqueous solution. Examples of the raw intensity are shown in 2D, Fig. 1, and 1D, Fig. 2, before being normalized and reduced to the structure function  $F(Q)$  then transformed to the PDF,  $G(r)$ . The  $F(Q)$  and  $G(r)$  are shown for both the precipitated crystalline API and the aqueous solution in Fig. 3. These can be considered as controls which establish the nature of the PDF for these constituents. Persistence of the signal out to high- $r$  (around 90 Å) for the crystalline control is due to its well ordered periodicity giving long-range coherence. The signal finally drops off due to the finite reciprocal-space resolution of the measurement. Meanwhile, the signal from the aqueous solvent disappears well before  $r = 20$  Å, because there is no structural coherence beyond the intramolecular bonding of the solution molecules and some near neighbor packing. This signal was measured with good statistics, as evident by minimal noise in the  $F(Q)$ , allowing its use as a background subtraction to the sample data.

Over the course of the experiment, the non-size reduced API settled out of solution, precipitating out the crystalline form. Before being used as a control for the other suspension samples, this signal is scaled and superimposed over that of the bulk crystal for comparison in Fig. 4. It is clear that there is significant disparity between the two PDFs in the low- $r$  region, up to about  $r = 10$  Å. To explore the cause of this,

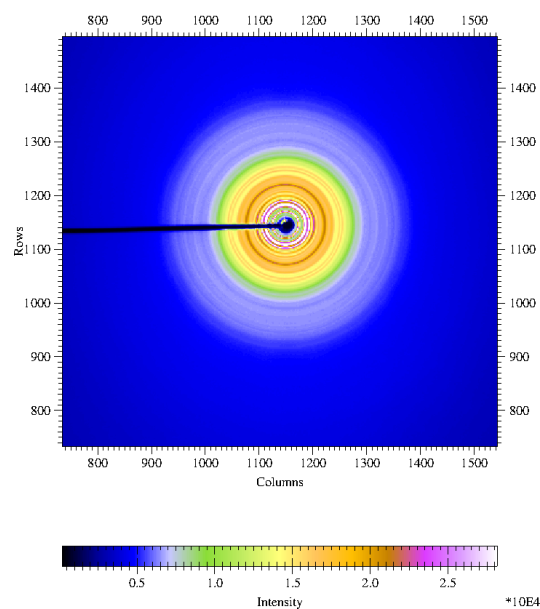


**Fig. 1** Example of raw data: microfluidized 5 wt. % sample on the 2D detector before integrating to get the 1D pattern.

the difference is taken between the scaled data sets, shown as the red line offset below the data curves. Plotted on top in light blue is the PDF of the aqueous solution which has been rescaled to have the same amplitude. The agreement is very good, in this case showing that the discrepancies between the two sample measurements do not come from irreproducibilities between data sets, but the fact that the precipitated API was still embedded in solution. Note that because the solvent signal is flat in the high- $r$  region, there is excellent reproducibility in the signals beyond 10 Å, even before subtraction as seen in Fig. 5. This illustrates the useful fact that a crystalline, or as will be shown later, a nanocrystalline component can be easily seen in the PDF, even in the presence of significant liquid or amorphous components.

While the non-size reduced API fell out of suspension and recrystallized, the microfluidized API at 5 wt. % did not. In this sample, the signal is dominated by 95 wt. % solvent. This is shown in Fig. 6(a), where the PDF is plotted overlaid by a scaled plot of the pure solvent. The curves are very similar, albeit with small deviations evident. A dPDF approach is taken to extract the signal coming from the micronized API in suspension by subtracting the scaled solvent background. Fig. 6(b) shows the PDFs, where signals from both 5 wt. % micronized suspension and the pure solvent are plotted over a wide range of  $r$ , with the difference curve plotted below in red. A signal is clearly visible extending to around 70–80 Å which presumably comes from the API in suspension. In order to

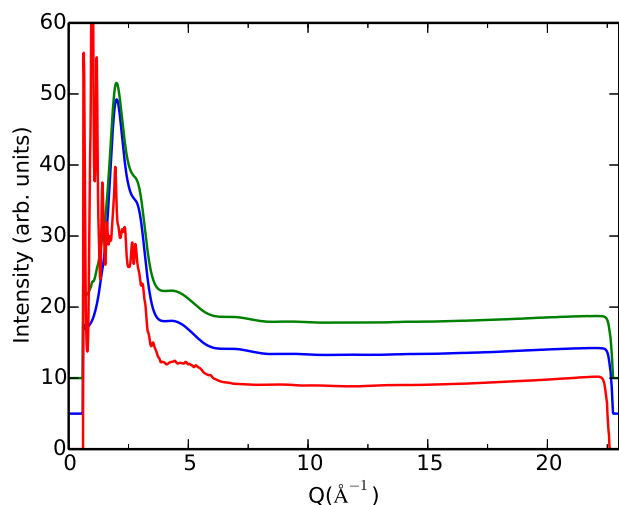


**Fig. 2** Integration of measured intensity: 1D raw signal after integration of Debye-Scherrer rings, Fig. 1, for precipitated crystalline API (red), aqueous solvent (blue), and 0.25 wt. % API suspension (green). Curves are offset for clarity.

confirm that the signal in the dPDF originates from the API, it is compared to the PDF of the precipitate recrystallized from solution with the same concentration in Fig. 7, with solution subtracted as shown necessary in Fig. 4. It is clear that the dPDF signal from the size-reduced suspension is the same as that from the crystalline API giving clear confirmation that this dPDF method is able to detect the presence of the API signal in suspension, even at 5 wt. % concentrations. In order to achieve this level of agreement, the signal from the crystalline precipitate was corrected for finite domain size effects. It was multiplied by the characteristic function for a sphere (Eq. 3) of diameter 16.9 nm. The diameter was estimated by carrying out a least-squares fit such that  $d$  was allowed to vary until the PDFs of the nanoparticles and size-corrected crystalline data gave the best agreement.

Sensitivity analysis is carried out to see how dilute the API can be while still remaining visible in the measured PDF. To do this, further diluted concentrations of 0.66 and 0.25 wt. % are considered. As concentrations become more dilute, it is increasingly challenging to detect a contribution that is statistically different from the blank with PDF methods. As seen in Fig. 2, the raw intensity from the solvent and 0.25 wt. % suspension are nearly indistinguishable. However, the question is whether any signal can be detected in the data after processing to obtain the fully corrected  $F(Q)$  and PDF,  $G(r)$ , functions. The resulting dPDFs are compared in Fig. 8. With decreasing API concentrations, there is an increasing presence of noise in the dPDF, as the API now accounts for less than one percent of the total signal. However, it is clear that as the

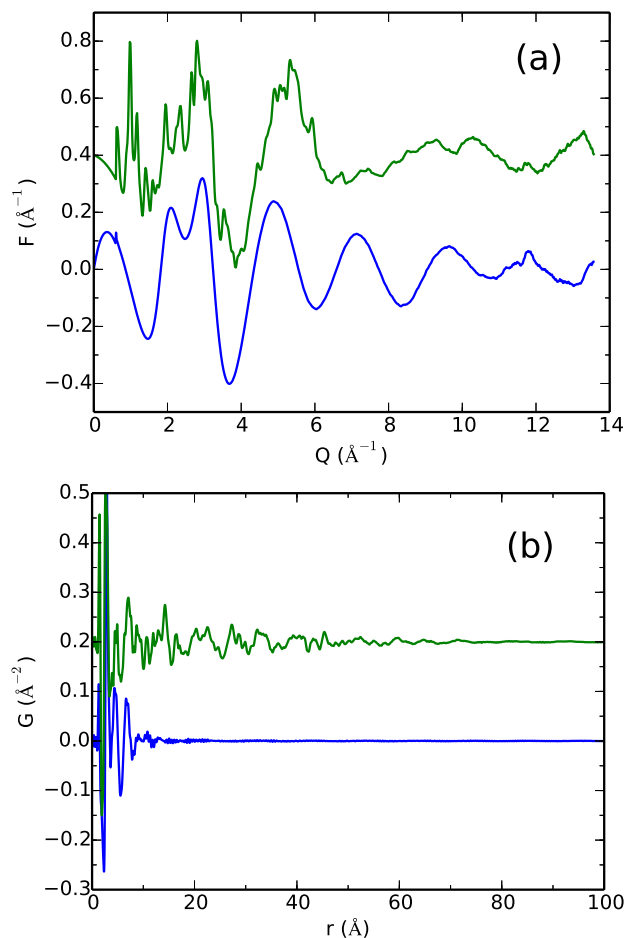


**Fig. 3** Representative data sets from control samples: precipitated crystalline API (green) and aqueous solvent (blue). (a)  $F(Q)$  (b) the PDF,  $G(r)$ .

concentration is reduced down to 0.25 wt. %, the structural signal from the API is still highly reproducible out to high- $r$ . While no structural model is available for the API, agreement with the crystalline form shows that quantitative analyses of the dPDF data from the dilute API is possible. To further explore this, a peak fitting algorithm<sup>51</sup> was used to extract peak positions and a baseline from the PDF of the domain-size corrected crystalline standard PDF. Gaussian functions were then fit to the crystalline and 0.25 wt. % PDFs at these positions, see Fig. 9. This constitutes a less highly constrained fit than would be the case in a real PDF structural refinement such as carried out with programs such as PDFfit<sup>52</sup> or PDFgui<sup>53</sup> and so is a strict test of the reliability of extracting quantities from the PDF of the dilute sample. Though there is higher uncertainty associated with the dilute suspension PDF due to the small signal, the peak positions from the crystal adequately

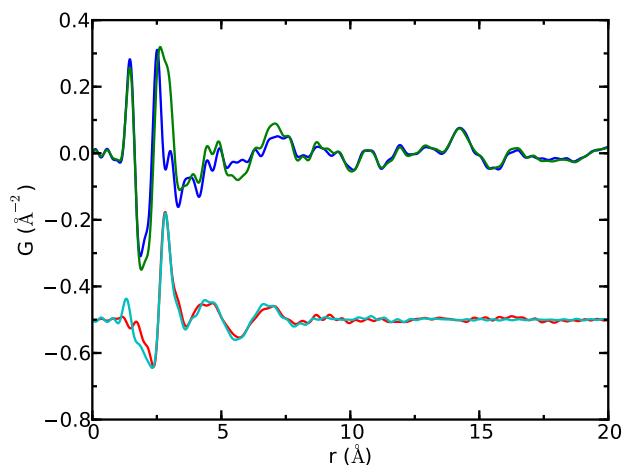


**Fig. 4** Comparison of bulk versus precipitated crystalline samples: PDFs from the bulk crystalline API (blue) and the crystalline API that precipitated from solvent (green). The PDF signals are subtracted (red) and compared to that of the aqueous solvent (light blue) with very good agreement showing that the only difference between the signals is the presence of significant solvent scattering in the latter case. PDF is sensitive to the presence or absence of residual solvent in the crystalline API.

account for all signal arising from the structure in the dilute PDF (Fig. 9) and values for peak widths and intensities match well, see Table 1.

Though PDFs from a wide variety of materials and at a varying range of diluted concentrations have been measured, few have reported on the actual sensitivity limits of the technique for their respective systems. One systematic study by Peterson et al.<sup>22</sup> reported phase determination with PDF to be accurate down to at least 2.5 wt. % and lower with single data set standards available. In the present case, single data set standards are utilized, and much lower component concentrations are analyzed, in our case with components which scatter far more weakly than do typical inorganics. As previously discussed, the limit of detection will depend on the particular situation in a dPDF study. For example, it is easier to detect the signal from a nanoparticle on the background of a liquid or amorphous host than it would be to detect a minority crystalline component in another crystalline material.

Detection at very dilute concentrations with PDF means that more components can be studied in their native environments, i.e., *in situ*, rather than in contrived situations with exaggerated concentrations. This is important, for example where aggregation of higher concentrations is an issue. Also, dilute samples can benefit time and cost when the primary component is rare or expensive. Better resolution can be expected in identifying

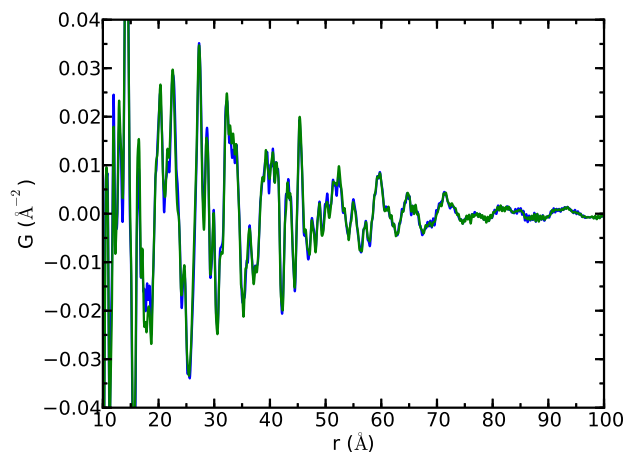


**Fig. 5** High- $r$  comparison of bulk versus precipitated crystalline samples: scaled to highlight the signal from the intermediate-range molecular packing in the crystal, from the bulk crystalline API (blue) and the crystalline API that precipitated from solvent (green). The figure illustrates the level of reproducibility that may be obtained by measuring two different samples of the same material.

consumption and production of components in reactive systems so that kinetic behavior can be studied. In the present case, the API can be studied at the actual concentration of the marketed drug product.

### 3 Conclusions

This work reports the sensitivity of the PDF to the presence of small quantities of crystalline or nanocrystalline components in a disordered matrix for a weakly scattering carbonaceous material. PDFs from quantities of nanocrystalline material as small as 0.25 wt. % could be extracted using difference methods from high quality synchrotron data that are suitable for quantitative analysis such as fingerprinting and structural modeling, even when the coherent domain size is only on the order of 10 nm. In terms of wt. % it is comparable to the reported state of the art for inorganic materials,<sup>49</sup> though much improved in terms of scattering power of the component of interest. The practicality of such a measurement is also improved using the latest data reduction methods. This will open doors to a multitude of studies such as crystalline and nanocrystalline APIs in amorphous matrix formulations (e.g. dispersion in polymer excipients), or inorganic nanoparticles embedded in a glass matrix, or in liquid suspensions as studied here.

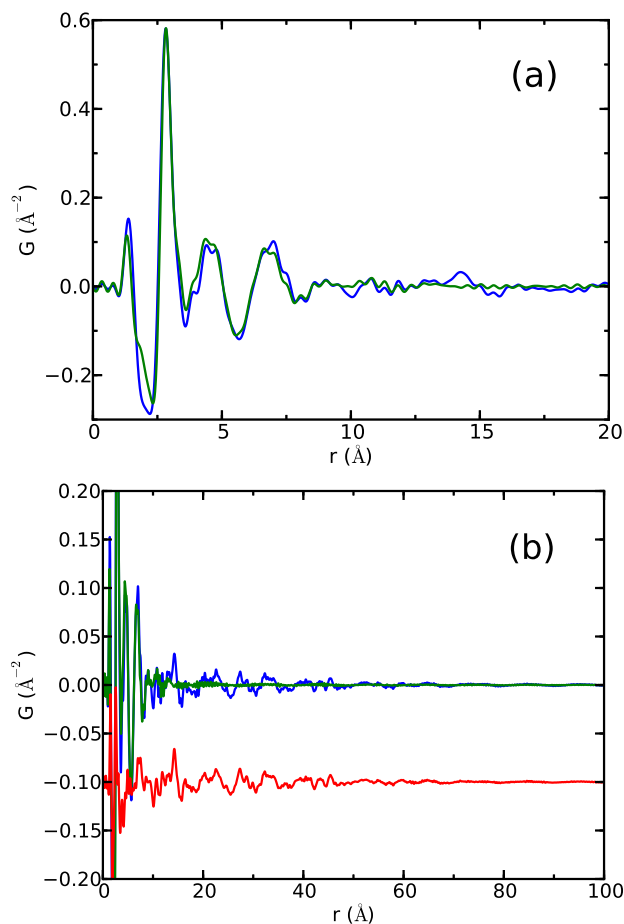


**Fig. 6** Comparison of precipitated and 5 wt. % suspension samples: PDFs from the 5 wt. % API (blue) and aqueous solvent (green). (a) Low- $r$  region of the PDF. (b) wide  $r$ -range with the difference of the PDF signals shown offset below (red).

## 4 Methods

### 4.1 PDF technique

The experimental PDF, denoted  $G(r)$ , is the truncated Fourier transform of the reduced total scattering structure function,  $F(Q) = Q[S(Q) - 1]$ ;<sup>54</sup>

$$G(r) = \frac{2}{\pi} \int_{Q_{\min}}^{Q_{\max}} F(Q) \sin(Qr) dQ, \quad (1)$$

where  $Q$  is the magnitude of the scattering momentum. The structure function,  $S(Q)$ , is extracted from the Bragg and diffuse components of X-ray, neutron or electron powder diffraction intensity. For elastic scattering,  $Q = 4\pi \sin(\theta)/\lambda$ , where  $\lambda$  is the scattering wavelength and  $2\theta$  is the scattering angle. In practice, values of  $Q_{\min}$  and  $Q_{\max}$  are determined by the ex-

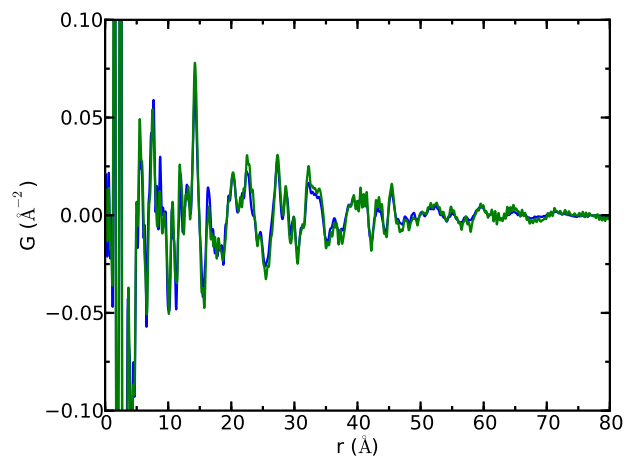


**Fig. 7** Determining the range of structural coherence for suspension particles: Reproducibility of the dPDF from the microfluidized 5 wt. % API obtained from reciprocal space subtraction of the suspension (green) and the crystalline precipitate corrected by a 16.9 nm domain size (blue).

perimental setup and  $Q_{\max}$  is often reduced below the experimental maximum to eliminate noisy data from the PDF since the signal to noise ratio becomes unfavorable in the high- $Q$  region.

For rapid fingerprinting of components, structural signals from measurement are overlaid and compared with a control sample.<sup>55</sup> This is useful for identifying the level of agreement in bonding motifs and structural coherence.<sup>12</sup> Atomic correlations can exist at very large distances for pristine crystalline samples, while they may only reach to the length of a single molecule for amorphous samples.

In the case of nanoparticles, this size effect is quantitatively accounted for by modulating an infinitely periodic crystalline PDF signal with a characteristic function  $\gamma(r)$ <sup>12,56</sup> to produce a new signal,

$$G_{\text{nano}}(r) = \gamma(r)G_{\infty}(r), \quad (2)$$

that reflects the expected attenuation with increasing- $r$  due to the effects from finite size and shape of the nanostructural domain of coherence. This domain may be much smaller than the nanoparticle in cases where there is significant structural disorder. The characteristic function for a sphere is

$$\gamma(r)_{\text{sphere}} = \left[ 1 - \frac{3r}{2d} + \frac{1}{2} \left( \frac{r}{d} \right)^3 \right] H(d - r), \quad (3)$$

where  $d$  is the domain diameter.  $H(r)$  is a step function with value 1 for  $r \leq d$  and 0 beyond.<sup>57</sup> It is useful to note that the signal is additionally attenuated by the finite resolution of the measurement.<sup>12</sup>

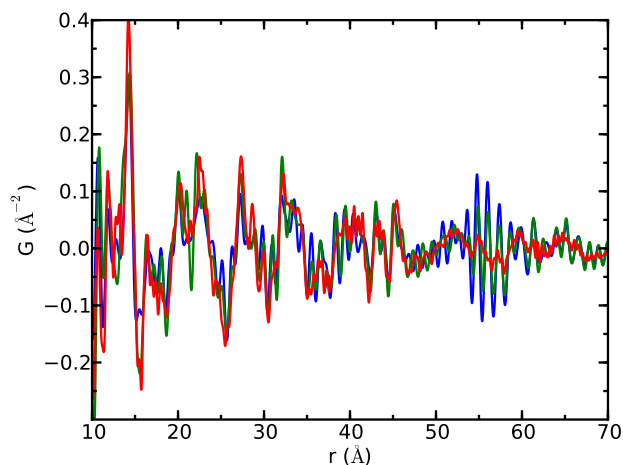


**Fig. 8** Signal sensitivity: dPDFs from reciprocal space subtraction of the solvent for the 0.25 (blue), 0.66 (green) and 5 (red) wt. % API samples. Despite increased noise ripples in the low concentration samples, the signal from the API is clearly evident.

The difference PDF method works because the measured PDF for a multi-phase material is a linear combination of the PDFs from each separate phase  $p$ ,

$$G(r) = \sum_p G_p(r). \quad (4)$$

This holds true if there is no structural coherence between the phases, which is a good approximation in most cases, except for example a phase that is toptaxially embedded in a crystalline matrix. This approximation works well for nanoparticles embedded in a glass or suspended in solvent, or incoherent mixtures of multiple phases in a powder or polycrystalline material. In this case, the contribution to the total from each phase is proportional to its relative concentration.

In general, the dPDF experiment is carried out in similar fashion to a typical powder X-ray diffraction experiment, though powder may refer to any form of the material of interest with the sole requirement that it is isotropic (e.g. crystalline or nanocrystalline powders, glasses, rubbery and waxy polymers, plastics, gels, liquid and amorphous colloids, solutions etc.). The high  $Q_{max}$  requirement means that the use of high energy, short wavelength synchrotron radiation is optimal, though molybdenum or silver anode radiation sources are also acceptable if given sufficient exposure time. The length of exposure, or time over which diffracted radiation is collected is significantly reduced by use of a 2D detector, the rapid acquisition PDF, (RAPDF) method,<sup>58</sup> but still intimately depends on the brilliance of the light source and diffracted intensity of the components in the sample. In certain cases, better statistics for the subtracted measurement may

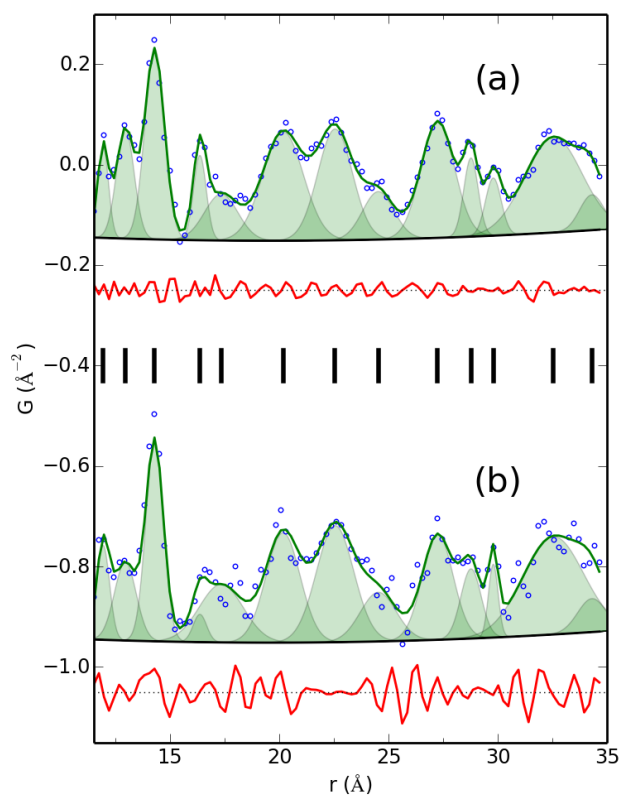


**Fig. 9** Peak fitting: PDF models are generated and compared by fitting Gaussian curves (light green) and a PDF baseline (black) at the extracted peak positions (black hash marks) to the data plotted on a Nyquist grid (blue) for (a) the crystalline standard, and (b) the 0.25 wt. % suspension. Differences are plotted in red.

be required to ensure that false correlations are not created due to noise at lower  $Q$  values for more weakly scattering background components when taking the difference. For a proper dPDF, this background measurement must include all undesirable scattering contributions: peripheral components, sample container, and even air scattering that occurs along the beam path. This should all be accounted for in a single measurement because attempts to separately measure them would result in redundant subtractions.

Measurements can be performed in a number of geometries, but for nanoparticles and solvents, it is convenient to measure samples loaded into sealed capillaries made of weakly scattering material such as polyimide or borosilicate. Once the raw intensity is measured for the total sample and the background components, the 2D data should be corrected for various effects such as polarization and experimental geometry,<sup>12</sup> then integrated to 1D intensity versus  $2\theta$  or  $Q$ , with software such as Fit2D.<sup>59</sup> Additional software, such as PDFGETX3, is available for the transformation step. The dPDF is gener-

**Table 1** Peak positions extracted from the crystalline standard PDF with height  $A_i$  and width (standard deviation)  $\sigma_i$  obtained by fitting Gaussian functions,  $G(r) = \sum_i A_i \exp\left(\frac{-(r-r_i)^2}{2\sigma_i^2}\right)$ , onto the baseline for both the standard (stan.) and 0.25 wt. % suspension (susp.) PDFs.

Position (Å)	height (Å <sup>-2</sup> )		width (Å)	
	stan.	susp.	stan.	susp.
11.92	0.18(1)	0.19(3)	0.25(2)	0.30(5)
12.94	0.22(1)	0.16(2)	0.40(3)	0.50(7)
14.28	0.38(1)	0.40(1)	0.44(1)	0.40(3)
16.36	0.17(1)	0.06(3)	0.29(3)	0.31(18)
17.34	0.092(7)	0.12(1)	0.77(13)	1.01(22)
20.17	0.22(1)	0.22(2)	0.93(6)	0.79(10)
22.55	0.22(1)	0.23(2)	0.79(4)	0.86(10)
24.53	0.095(8)	0.10(2)	0.72(10)	0.82(23)
27.25	0.23(1)	0.21(2)	0.76(5)	0.70(10)
28.77	0.16(1)	0.14(2)	0.33(3)	0.47(11)
29.80	0.11(1)	0.15(3)	0.36(5)	0.22(6)
32.54	0.190(7)	0.19(2)	1.31(8)	1.39(17)
34.31	0.07(1)	0.07(2)	0.55(11)	0.65(33)

ated prior to this step by subtracting the integrated intensity of the background from the total intensity measurement, typically scaled by the ratio of total photon counts, or the total exposure time, from each measurement. The output is then normalized to generate  $S(Q)$ ,  $F(Q)$ , and the dPDF,  $G(r)$ . For dPDF calculation, the subtraction should occur in reciprocal space rather than real space because systematic errors between data set transformations can have deleterious effects on the resulting PDF, particularly in cases of minute component concentrations.

## 4.2 Experiments

The experiments were carried out at beamline ID15 at the European Synchrotron Radiation Facility (ESRF) using the RAPDF method. A 2D Perkin Elmer detector was placed at a distance of 160 mm from the samples which were loaded in 2 mm ID Kapton capillaries. Data were collected at 300 K. The incident energy of the X-rays was 55.634 keV corresponding to a wavelength of  $\lambda = 0.22286$  Å. Calibration of the experimental setup was done using CeO<sub>2</sub> as a standard. Exposure time was adjusted for each sample to avoid detector saturation, and the number of frames taken for each sample was adjusted to obtain sufficient counting statistics on the data, 10 minutes for crystalline samples and 27 minutes for suspension samples.

Raw data as depicted in Fig. 1 were summed and corrected for polarization effects then integrated along arcs of constant scattering angle to produce 1D powder diffraction patterns,

Fig. 2, using the program Fit2D. Corrections and normalizations to the data were then carried out to obtain the total scattering structure function,  $F(Q)$ , which was Fourier transformed to obtain the PDF using the program PDFGETX3. The maximum momentum transfer used in the Fourier transform,  $Q_{max}$ , was varied to maximize information content while minimizing noise at high- $Q$  which can have adverse effects on structural features at low- $r$  in the PDF.

## 5 Acknowledgements

The authors thank M. Jamieson for help with the manuscript and acknowledge the ESRF for the award of in-house experimental time. Work in the S.J.L.B. group was supported by the Laboratory Directed Research and Development (LDRD) program 12-007 (Complex Modeling) at Brookhaven National Laboratory (BNL) which is supported by the Office of Science, US Department of Energy (OS-DOE), under Contract No. DE-SC00112704. M.T. was partially supported by the Columbia University Energy Frontier Research Center (EFRC) funded by the U.S. Department of Energy, Basic Energy Sciences (DOE-BES), under Grant No. DE-SC0001085.

## References

- 1 C. Tyrsted, K. M. Ø. Jensen, E. D. Bøjesen, N. Lock, M. Christensen, S. J. L. Billinge and B. B. Iversen, *Angew. Chem. Int. Edit.*, 2012, **51**, 9030–9033.
- 2 V. R. Patel and Y. K. Agrawal, *J. Adv. Pharm. Technol. Res.*, 2011, **2**, 81–87.
- 3 H. S. Choi and J. V. Frangioni, *Mol. Imaging*, 2010, **9**, 291–310.
- 4 C. T. J. Low, R. G. A. Wills and F. C. Walsh, *Surf. Coat. Tech.*, 2006, **201**, 371–383.
- 5 A. Nawrocka and J. Ciesla, *Int. Agrophysics*, 2013, **27**, 49–55.
- 6 S. Vafaei and D. Wen, *Heat Mass Transfer*, 2012, **48**, 349–357.
- 7 S. A. Claridge, A. W. C. Jr., S. N. Khanna, C. B. Murray, A. Sen and P. S. Weiss, *ACS Nano*, 2009, **3**, 244–255.
- 8 K. D. Hermanson, S. O. Lumsdon, J. P. Williams, E. W. Kaler and O. D. Velev, *Science*, 2001, **29**, 1082–1086.
- 9 M. Murawska, A. Skrzypczak and M. Kozak, *Acta Phys. Pol. A*, 2012, **121**, 888–892.
- 10 M. Zimbone, L. Calcagno, G. Messina, P. Baeri and G. Compagnini, *Mater. Lett.*, 2011, **65**, 2906–2909.
- 11 J. E. Evans, K. L. Jungjohann, N. D. Browning and I. I. Arslan, *Nano Lett.*, 2011, **11**, 2809–2813.
- 12 T. Egami and S. J. L. Billinge, *Underneath the Bragg peaks: structural analysis of complex materials*, Elsevier, Amsterdam, 2nd edn, 2012.
- 13 K. Page, T. Proffen, H. Terrones, M. Terrones, L. Lee, Y. Yang, S. Stemmer, R. Seshadri and A. K. Cheetham, *Chem. Phys. Lett.*, 2004, **393**, 385–388.
- 14 V. Petkov, T. Ohta, Y. Hou and Y. Ren, *J. Phys. Chem. C*, 2007, **111**, 714–720.
- 15 C. Shi, E. L. Redmond, A. Mazaheripour, P. Juhás, T. F. Fuller and S. J. L. Billinge, *J. Phys. Chem. C*, 2013, **117**, 7226–7230.
- 16 V. Petkov, Y. Ren, S. Shan, J. Luo and C.-J. Zhong, *Nanoscale*, 2014, **6**, 532–538.

- 17 B. Gilbert, F. Huang, H. Zhang, G. A. Waychunas and J. F. Banfield, *Science*, 2004, **305**, 651–654.
- 18 A. S. Masadeh, E. S. Božin, C. L. Farrow, G. Paglia, P. Juhás, A. Karkamkar, M. G. Kanatzidis and S. J. L. Billinge, *Phys. Rev. B*, 2007, **76**, 115413.
- 19 X. Yang, A. S. Masadeh, J. R. McBride, E. S. Božin, S. J. Rosenthal and S. J. L. Billinge, *Phys. Chem. Chem. Phys.*, 2013, **15**, 8480–8486.
- 20 P. Juhás, D. M. Cherba, P. M. Duxbury, W. F. Punch and S. J. L. Billinge, *Nature*, 2006, **440**, 655–658.
- 21 T. Proffen, K. L. Page, S. E. McLain, B. Clausen, T. W. Darling, J. A. TenCate, S.-Y. Lee and E. Ustundag, *Z. Kristallogr.*, 2005, **220**, 1002–1008.
- 22 J. Peterson, J. TenCate, T. Proffen, T. Darling, H. Nakotte and K. Page, *J. Appl. Crystallogr.*, 2013, **46**, 332–336.
- 23 C. J. Benmore, J. K. R. Weber, A. N. Taylor, B. R. Cherry, J. L. Yarger, Q. Mou, W. Weber, J. Neufeind and S. R. Byrn, *J. Pharm. Sci.*, 2013, **102**, 1290–1300.
- 24 T. Davis, M. Johnson and S. J. L. Billinge, *Cryst. Growth Des.*, 2013, **13**, 42394244.
- 25 R. Harrington, D. B. Hausner, N. Bhandari, D. R. Strongin and K. W. Chapman, *Inorg. Chem.*, 2010, **49**, 325–330.
- 26 P. J. Chupas, K. W. Chapman and G. J. Halder, *J. Am. Chem. Soc.*, 2011, **133**, 8522–8524.
- 27 K. Page, T. C. Hood, T. Proffen and R. B. Neder, *J. Appl. Crystallogr.*, 2011, **44**, 327–336.
- 28 W. Li, R. Harrington, Y. Tang, J. D. Kubicki, M. Aryanpour, R. J. Reeder, J. B. Parise and B. L. Phillips, *Environ. Sci. Technol.*, 2011, **45**, 9687–9692.
- 29 V. Petkov, S. J. L. Billinge, T. Vogt, A. S. Ichimura and J. L. Dye, *Phys. Rev. Lett.*, 2002, **89**, 075502.
- 30 K. W. Chapman, P. J. Chupas and C. J. Kepert, *J. Am. Chem. Soc.*, 2005, **127**, 11232–11233.
- 31 K. W. Chapman, P. J. Chupas, E. R. Maxey and J. W. Richardson, *Chem. Commun.*, 2006, 4013–4015.
- 32 H. Kim, A. Karkamkar, T. Autrey, P. Chupas and T. Proffen, *J. Am. Chem. Soc.*, 2009, **131**, 13749–13755.
- 33 P. J. Chupas, K. W. Chapman, G. Jennings, P. L. Lee and C. P. Grey, *J. Am. Chem. Soc.*, 2007, **129**, 13822–13824.
- 34 H. Zhao, T. M. Nenoff, G. Jennings, P. J. Chupas and K. W. Chapman, *J. Phys. Chem. Lett.*, 2011, **2**, 2742–2746.
- 35 C. Tyrsted, B. R. Pauw, K. M. O. Jenson, J. Becker, M. Christensen and B. B. Iversen, *Chem.-Eur. J.*, 2012, **18**, 5759–5766.
- 36 H. Zhao, P. J. Chupas and K. W. Chapman, *Z. Kristallogr.*, 2012, **227**, 268–271.
- 37 K. M. Ø. Jensen, M. Christensen, P. Juhás, C. Tyrsted, E. D. Bøjesen, N. Lock, S. J. L. Billinge and B. B. Iversen, *J. Am. Chem. Soc.*, 2012, **134**, 6785–6792.
- 38 Y. Lei, J. Lu, H. Zhao, B. Liu, K.-B. Low, T. Wu, J. A. L. and Jeffrey P. Greeley, P. J. Chupas, J. T. Miller and J. W. Elam, *J. Phys. Chem. C*, 2013, **117**, 11141–11148.
- 39 J. Keating, G. Sankar, T. I. Hyde, S. Kohara and K. Ohara, *Phys. Chem. Chem. Phys.*, 2013, **15**, 8555–8565.
- 40 S. J. Smith, S. Amin, B. F. Woodfield, J. Boerio-Goates and B. J. Campbell, *Inorg. Chem.*, 2013, **52**, 4411–4423.
- 41 C. E. White, J. L. Provis, A. Llobet, T. Proffen and J. S. J. van Deventer, *J. Am. Ceram. Soc.*, 2011, **94**, 3532–3533.
- 42 M. A. Newton, K. W. Chapman, D. Thompsett and P. J. Chupas, *J. Am. Chem. Soc.*, 2012, **134**, 5036–5039.
- 43 B. Shyam, K. W. Chapman, M. Balasubramanian, R. J. Klingler, G. Srajer and P. J. Chupas, *Angew. Chem. Int. Edit.*, 2012, **51**, 4852–4855.
- 44 C. E. White, J. L. Provis, B. Bloomer, N. J. Henson and K. Page, *Phys. Chem. Chem. Phys.*, 2013, **15**, 8573–8582.
- 45 E. L. Redmond, B. P. Setzler, P. Juhás, S. J. L. Billinge and T. F. Fuller, *Electrochem. Solid St.*, 2012, **15**, B72–B74.
- 46 K. M. Wiaderek, O. J. Borkiewicz, E. Castillo-Martinez, R. Robert, N. Pereira, G. G. Amatucci, C. P. Grey, P. J. Chupas and K. W. Chapman, *J. Am. Chem. Soc.*, 2013, **135**, 4070–4078.
- 47 D. L. Price and M.-L. Saboungi, *Local Structure from Diffraction*, New York, 1998, p. 23.
- 48 Y. Waseda, *Novel Applications of Anomalous (Resonance) X-ray Scattering for Structural Characterization of Disordered Materials*, Springer-Verlag, Berlin, 1984.
- 49 A. Gagin, A. J. Allen and I. Levin, *J. Appl. Crystallogr.*, 2014, **47**, 619–629.
- 50 P. Juhás, T. Davis, C. L. Farrow and S. J. L. Billinge, *J. Appl. Crystallogr.*, 2013, **46**, 560–566.
- 51 L. Granlund, S. J. L. Billinge and P. M. Duxbury, *Acta Crystallogr. A*, submitted, 2014.
- 52 T. Proffen and S. J. L. Billinge, *J. Appl. Crystallogr.*, 1999, **32**, 572–575.
- 53 C. L. Farrow, P. Juhás, J. Liu, D. Bryndin, E. S. Božin, J. Bloch, T. Proffen and S. J. L. Billinge, *J. Phys: Condens. Mat.*, 2007, **19**, 335219.
- 54 C. L. Farrow and S. J. L. Billinge, *Acta Crystallogr. A*, 2009, **65**, 232–239.
- 55 S. J. L. Billinge, T. Dykhne, P. Juhás, E. Božin, R. Taylor, A. J. Florence and K. Shankland, *CrystEngComm*, 2010, **12**, 1366–1368.
- 56 K. Kodama, S. Iikubo, T. Taguchi and S. Shamoto, *Acta Crystallogr. A*, 2006, **62**, 444–453.
- 57 A. Guinier, G. Fournet, C. Walker and K. Yudowitch, *Small-angle scattering of x-rays*, John Wiley & Sons, Inc., New York, 1955.
- 58 P. J. Chupas, X. Qiu, J. C. Hanson, P. L. Lee, C. P. Grey and S. J. L. Billinge, *J. Appl. Crystallogr.*, 2003, **36**, 1342–1347.
- 59 A. P. Hammersley, S. O. Svenson, M. Hanfland and D. Hauserman, *High Pressure Res.*, 1996, **14**, 235–248.